On the relationship between crack initiation angle and loading equivalent angle for asymmetric Three-Point Bend Specimens under mixed-mode I/II loading based on GMPZR criterion

Mujebur Rehaman
Department of Mechanical Engineering, PES Institute of Technology & Management, Shivamogga 577204, Visvesvaraya Technological University, Belagavi, India.
mujebur.rehaman@pestrust.edu.in

Manjunath Patel G C
Department of Mechanical Engineering, Sahyadri College of Engineering & Management, Mangaluru 575007, Visvesvaraya Technological University, Belagavi, India.
manjunath.me@sahyadri.edu.in

Mohan T R
Department of Mechanical Engineering, Bapuji Institute of Engineering and Technology, Davangere -577004, Visvesvaraya Technological University, Belagavi, India.
mohantrdvg@gmail.com

S K Kudari
National Institute of Technology Goa, Cuncolium, South Goa District Goa 403 703, India
s.kudari@rediffmail.com

Sharnaprabhu C M
Department of Mechanical Engineering, PES Institute of Technology & Management, Shivamogga 577204, Visvesvaraya Technological University, Belagavi, India.
cmsharanaprabhu@rediffmail.com

ABSTRACT. In this work, the prediction of crack initiation angle (θ_o) under mixed mode (I/II) load is estimated from the generalized minimum plastic zone radius (GMPZR) criterion. The paper presents a detailed study on the crack-tip plastic core for asymmetric three-point bend (TPB) specimens of

OPEN ACCESS

Citation: Rehman, M., Patel, M. G. C., Mohan, T. R., Kudari, S. K., Sharnaprabhu, C. M., On the relationship between crack initiation angle and loading equivalent angle for asymmetric Three-Point Bend Specimens under mixed-mode I/II loading based on GMPZR criterion, Fracture and Structural Integrity, 77 (2026) 45-55.

Received: 05.01.2026
Accepted: 31.03.2026
Published: 04.04.2026
Issue: 07.2026

different crack-to-width (a/W) = 0.4-0.7 ratios and loading equivalent angle (β_{eq}) using elastic finite element (FE) analyses. The θ_o estimated from the FE analysis is compared with the GMPZR criterion, other fracture criteria, and available experimental results. It is found that the θ_o evaluated from the FE analysis provides the best correlation with the GMPZR criterion among other fracture criteria. The FE results are used to propose an analytical relation between θ_o and β_{eq}. This proposed relationship can be used to quickly estimate the crack initiation direction/angle for TPB specimens with only β_{eq} available. Finally, the effect of T-stress on θ_o, will be assessed using as estimated from the GMPZR criterion.

KEYWORDS. Three-point bend specimen, Crack initiation angle, Finite element analysis.

INTRODUCTION

The multifarious nature of the real loading condition ahead of the crack tip for service-manufacturing components under combined (Mode I & Mode II) conditions is linked to the estimation of crack/fracture initiation [1]. Preventing catastrophic failure in industrial components requires the precise measurement and prediction of the crack initiation angle and direction [2]. The predictions of crack initiation for structures/components were analyzed using several fracture criteria [3] based on the fracture parameters such as the stress intensity factor, J-integral, and crack tip opening displacement [4, 5]. The researchers [6] proposed various fracture criteria by considering a constant core radius around the crack tip, known as the plastic zone (PZ), which occurs from the localization of stress amplitude for analyses of fracture initiation/direction. However, the PZ was not constant near the crack tip, and Breitbarth et al. reported that the fracture initiation occurs where the PZ is smallest [7]. Later, based on the PZ size and shape near the crack tip derived from the von Mises yield criterion [8], Bian and Kim [9] proposed the minimum plastic zone radius (MPZR) criterion. They [9, 10] showed that the crack initiation angle (θ_o) for mixed-mode loading occurs at the point where the PZ radius attains a global minimum ahead of the crack tip. Subsequently, detailed finite element analyses were performed to measure the crack initiation based on the MPZR criterion ahead of the crack tip under mixed-mode (I/II) loading. Accordingly, researchers [11] numerically analyzed the estimation of crack initiation by considering the shape and size of a PZ ahead of the crack tip derived from the von Mises yield criterion. Furthermore, many investigators [12, 13] used a non-dimensional applied load parameter, the loading equivalent angle ($\beta_{eq} = tan^{-1}(K_I/K_{II})$), to determine crack initiation under mixed-mode (I/II) loading. Next, improvements in crack-prediction models for structures/components can be achieved by considering the second term in the stress field around the crack tip. Related to the second term, or non-singular parameter (T-stress), many researchers [12, 14] have recognized that the effect of the second term of the Williams Series on the plastic core and on the crack growth direction/initiation is significant. Shahani and Tabatabaei [12] numerically extracted T-stress from the FE software tool for an asymmetric four-point bend fracture specimen and suggested that the T-stress would affect the different fracture criteria [15]. However, the theoretical fracture criteria do not include the T-stress term in the analysis. Ayatollahi et al. [16] demonstrated a generalized maximum tensile stress criterion by considering T-stress for predicting the crack initiation under combined tensile and shear (mixed mode) loading. The authors [16] numerically analyzed various asymmetric specimens and found that the generalized maximum tensile stress criterion yields better results than the maximum tensile stress criterion. In addition, Nazarali and Wang [17] studied the effects of T-stress on the plastic zone ahead of the crack tip under mixed-mode (I/II) loading conditions and suggested that T-stress is an important parameter for fatigue and fracture analyses to identify defects in structures. Miao et al. [18] numerically analyzed the effect of T-stress on plastic zone for various mixed-mode (I/II) fracture specimens and recommended that the T-stress plays a significant role in crack initiation angle and plastic zone around the crack tip, which in turn can affect the fracture of the specimen. However, the examination of fracture initiation criteria based on PZ ahead of the crack tip, by considering stress intensity factors and T-stress to estimate the crack initiation direction under mixed-mode (I/II) loading conditions, was not available. Hence, the objectives of the present work are as follows i) A GMPZR criterion were carried out from stress intensity factors and T-stress parameters to estimate fracture initiation, which is extension of MPZR criterion, ii) the FE analyses were carried out on asymmetric TPB specimen for various a/W ratios and β_{eq} to analyze the size and shape of crack-tip PZ, iii) The crack

initiation angle estimated from FE analyses was compared with the proposed GMPZR fracture criterion, other theoretical fracture criteria and available experimental results, iv) from the FE analyses an attempt is been made to estimate approximate formulation for GMPZR and crack initiation angles based on stress intensity factors under mixed-mode (I/II) loading, and v) finally, the effects of T-stress on crack initiation angle estimated from GMPZR criterion were also studied

GENERALIZED MINIMUM PLASTIC ZONE RADIUS CRITERION

A generalized minimum plastic zone radius (GMPZR) criterion is an extension of the MPZR [9, 19] criterion. It states that the direction of crack initiation coincides with the direction of minimum plastic zone radius evaluated from the von Mises yield criterion. The radius of PZ ahead at the crack tip contains stress intensity factors and T-stress. The crack initiation can be determined by minimizing r [9, 19]:

$$\left(\frac{\partial r}{\partial \theta}\right)_{\theta=\theta_o} = 0 \qquad \left(\frac{\partial^2 r}{\partial \theta^2}\right)_{\theta=\theta_o} > 0 \tag{1}$$

The stresses near the crack tip expressed in terms of Cartesian co-ordinates (x, y) are given as:

$$\begin{Bmatrix}\sigma_{xx}\\ \sigma_{yy}\\ \tau_{xy}\end{Bmatrix} = \frac{K_I}{\sqrt{2\pi r}}\begin{Bmatrix}\cos\frac{\theta}{2}\left[1-\sin\left(\frac{\theta}{2}\right)\sin\left(\frac{3\theta}{2}\right)\right]\\ \cos\frac{\theta}{2}\left[1+\sin\left(\frac{\theta}{2}\right)\sin\left(\frac{3\theta}{2}\right)\right]\\ \cos\frac{\theta}{2}\sin\left(\frac{\theta}{2}\right)\cos\left(\frac{3\theta}{2}\right)\end{Bmatrix} + \frac{K_{II}}{\sqrt{2\pi r}}\begin{Bmatrix}\sin\left(\frac{-\theta}{2}\right)\left[2+\cos\left(\frac{\theta}{2}\right)\cos\left(\frac{3\theta}{2}\right)\right]\\ \cos\frac{\theta}{2}\sin\left(\frac{\theta}{2}\right)\sin\left(\frac{3\theta}{2}\right)\\ \cos\frac{\theta}{2}\left[1-\sin\left(\frac{\theta}{2}\right)\sin\left(\frac{3\theta}{2}\right)\right]\end{Bmatrix} + \begin{Bmatrix}T\\0\\0\end{Bmatrix} \tag{2}$$

$$\sigma_{zz} = \tau_{xz} = \tau_{yz} = 0 \qquad \text{Plane stress} \tag{3}$$

where K_I and K_{II} are the stress intensity factors in Mode I and Mode II, respectively.
The Von Mises yield criteria for a 3D object can be written in the following form

$$\left(\sigma_{xx}-\sigma_{yy}\right)^2+\left(\sigma_{yy}-\sigma_{zz}\right)^2+\left(\sigma_{zz}-\sigma_{xx}\right)^2 = 2\sigma_y^2 \tag{4}$$

One can substitute the singular stress field of Eq. (2) in the above yield criterion Eq. (4) and solve for the PZ radius r. It can be expressed as follows.

$$\begin{aligned} r(K_I,K_{II},T,\theta) = \frac{1}{4\sigma_y^2}\Bigg[& K_I^2\left\{\frac{3}{4}(1-\cos 2\theta)+2\cos^2\frac{\theta}{2}\right\}+K_{II}^2\left\{\frac{15}{4}+2\sin^2\frac{\theta}{2}+\frac{9}{4}\cos 2\theta\right\} \\ & +K_IK_{II}\left\{\frac{13}{4}\sin 2\theta+\frac{3}{8}\sin 3\theta-2\sin\theta\right\}\Bigg]+\left(\frac{T}{\sigma_y}\right)^2+\frac{K_IT\sqrt{2\pi r}}{2\sigma_y^2}\left(\frac{1}{2}\cos\frac{\theta}{2}+\frac{3}{2}\cos\frac{5\theta}{2}\right) \\ & -\frac{K_{II}T\sqrt{2\pi r}}{2\sigma_y^2}\left(\frac{13}{2}\sin\frac{\theta}{2}+\frac{3}{4}\sin\frac{5\theta}{2}\right) \end{aligned} \tag{5}$$

By substituting Eq. (5) in Eq. (1), we get,

$$\left.\frac{\partial r}{\partial\theta}\right|_{\theta=\theta_o}=\frac{K_I^2}{4\sigma_y^2}\left(\frac{3}{2}\sin 2\theta_o-\sin\theta_o\right)+\frac{K_{II}^2}{4\sigma_y^2}\left(\sin\theta_o-\frac{9}{2}\sin 2\theta_o\right)$$
$$+\frac{K_I K_{II}}{4\sigma_y^2}\frac{13}{2}\left(\cos 2\theta_o+\frac{9}{8}\cos 3\theta_o-2\cos\theta_o\right)-\frac{K_I T\sqrt{2\pi r}}{4\sigma_y^2}\left(\sin\frac{\theta_o}{2}+3\sin\frac{5\theta_o}{2}\right)$$
$$-\frac{K_{II}T\sqrt{2\pi r}}{4\sigma_y^2}\left(13\cos\frac{\theta_o}{2}+15\cos\frac{5\theta_o}{2}\right)=0 \qquad (6)$$

Eqn. (6) is used to determine the crack initiation /direction (θ_o) according to the GMPZR criterion.

FINITE ELEMENT ANALYSIS

The sequence of 2D stress analyses for the asymmetric TPB specimen was performed using ABAQUS. The asymmetric TPB specimen dimensions for the FE analyses are taken from the work of Shahani and Tabatabaei [12], as shown in Fig. 1. During FE analyses, the loading and boundary conditions for the asymmetric TPB specimen were similar to those reported by Ma *et al.* [20]. Due to asymmetric loading, the full specimen geometry is considered in the FE analyses. The meshing of the asymmetric TPB specimen is done using quadratic 2D Isoparametric solid elements. Researchers [16] utilized the quadratic 2D Isoparametric solid elements to extract *K* and *T* for the various specimens in the FE analyses. Fig. 2 shows a 2D FE mesh of the asymmetric TPB specimen used for the analyses. The asymmetric TPB specimen is analyzed for central loading position of a/W=0.4-0.7 ratios with an increment of 0.1 and for 6 different crack positions (s/L=0-1, where, s and L are shown in Fig. 1). The number of elements for these six different crack positions of the asymmetric TPB specimen are varies from 1500 to 2000. The ABAQUS post-processor has extracted the magnitudes of *K* and *T*. The procedure for computing *K* and *T* in the ABAQUS FE software tool uses the J-integral method [21] which is documented. Interstitial free steel (IF steel) was considered for the linear elastic FE analysis, which is used in car bodies due to its high formability [22]. The tensile properties of the material for FE analyses were extracted from earlier works [22], and they are: elastic modulus (E) = 197 GPa, yield strength (σ_y) = 155 MPa, Poisson's ratio (υ)=0.3.

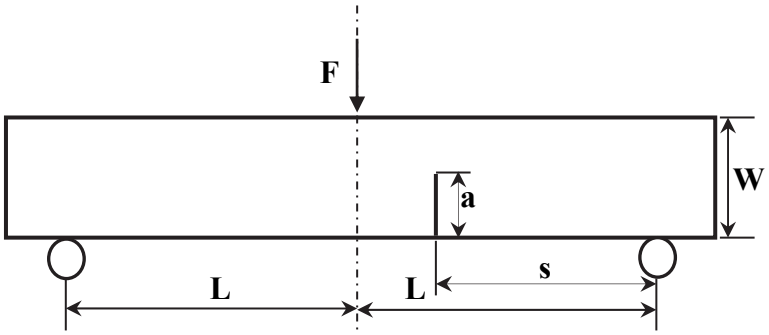

Figure 1: Specimen configuration used in the analysis be W = 30 mm, a = 15 mm, L = 86 mm, thickness (h) = 3 mm.

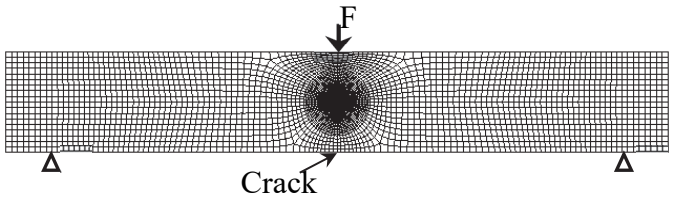

Figure 2: A typical 2D asymmetric TPB specimen FE mesh used in the analysis.

ANALYTICAL ESTIMATES OF STRESS INTENSITY FACTORS

The analytical formulation for the asymmetric three-point bend specimen is not available in the literature. The formulations proposed by He and Hutchinson [23] for estimating K for an asymmetric four-point bend specimen are used to modify for the asymmetric 3PB specimen as under:

$$K_I = \frac{3Qs}{bW^2}\sqrt{\pi a}\,F_I\left(\frac{a}{W}\right) \tag{7}$$

where, $3Qs/bW^2$ is the applied bending stress in the case of the 3PB specimen
Similarly,

$$K_{II} = \frac{Q(a/W)^{3/2}}{6bW^{1/2}(1-a/W)^{1/2}}F_{II}\left(\frac{a}{W}\right) \tag{8}$$

In the case of the 3PB specimen, $Q = F$
Q = Shear Force
where, b is the thickness of the specimen, a is the crack length, and W is the width of the specimen. The $Fi = (a/W)$ polynomial equations by Murakami [24]:

$$F_I\left(\frac{a}{W}\right) = 1.122 + 1.121(a/W) + 3.740(a/W)^2 + 3.873(a/W)^3 - 19.05(a/W)^4 + 22.5(a/W)^5$$
$$\text{for } 0 \le a/W \le 0.7 \tag{9}$$

$$F_{II}\left(\frac{a}{W}\right) = 7.264 - 9.37(a/W) + 2.74(a/W)^2 + 1.87(a/W)^3 - 1.04(a/W)^4$$
$$\text{for } 0 \le a/W \le 1 \tag{10}$$

Using the above equations, a C program has been developed to compute K_I and K_{II} for various applied loads.

RESULTS AND DISCUSSION

To estimate K, T, and to accomplish the contour and magnitude of PZ ahead of the crack-tip, various load steps were applied on an asymmetric TPB specimen of different a/W and β_{eq}. For different load steps and β_{eq}, the K and T for the asymmetric TPB specimen have been computed using the ABAQUS postprocessor. The analyses of K_I and K_{II} for each β_{eq} will be handled using the effective stress intensity factor (K_{eff}), given by $K_{eff} = \sqrt{K_I^2 + K_{II}^2}$. In the analyses, the K_{eff} will be normalized by yield stress and the square root of the thickness ($\sigma_y h^{1/2}$). The premeditated values of normalized K_{eff} for a/W = 0.4-0.7 in asymmetric TPB specimens, typically for a 1kN applied load, are plotted against β_{eq} in Fig. 3. The finite element analysis (FEA) results and theoretical results of normalized K_{eff} vs. β_{eq} show good agreement. The analytical values of K_{eff} for various load steps, a/W, and β_{eq} of the asymmetric TPB specimen have been calculated from Eqns. (7) and (8). The percentage error between the FEA and theoretical results is less than 3.5%. This error may be attributed to the varied s/L ratio and bend loading condition of the asymmetric TPB specimen. Fig. 3 demonstrates that the normalized K_{eff} increases as β_{eq} changes from 0^o (Mode II) to 90^o (Mode I), and for the same applied load, the normalized K_{eff} is almost 20 times higher for $\beta_{eq} = 90^o$ than for $\beta_{eq} = 0^o$. Also, Fig. 3 shows that normalized K_{eff} depends on a/W and the applied load. The T-stress will be evaluated using the dimensionless biaxiality ratio (B) $B = T\sqrt{\pi a}/K_{eff}$ and K_{eff} [12, 25]. The variation of B vs. a/W is shown in Fig. 4 for different β_{eq}. From Fig. 4, the computed B exactly matches Sham's [26] results for the TPB

specimen with β_{eq} = 90° (Mode I). *B* is negative for β_{eq} =0° and it is positive for the remaining β_{eq} values, for a/W =0.4 to 0.7. The Fig. 4 clearly shows that B is almost constant for β_{eq} = 75° to 86° with a/W ratios of 0.4 to 0.7 ratios.

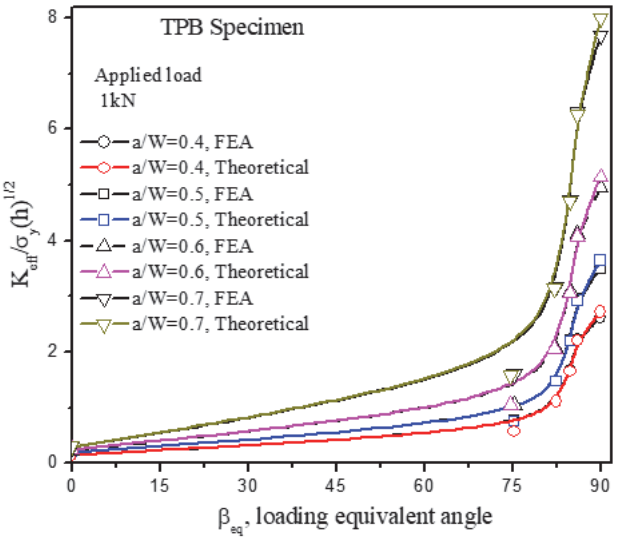

Figure 3: Specimen Comparison of FE and Analytical results of $K_{eff}/\sigma_y(h)^{1/2}$ *vs.* β_{eq} for various a/W.

The studies on the magnitudes and contours of the PZ ahead of a crack tip were considered for various β_{eq} values in an asymmetric TPB specimen. The contours of the PZ were determined by plotting iso-contours based on the von Mises criterion, using the materials yield stress. Since an elastic constitutive model is used for the material, contour plots of the von Mises stress show the PZ shape. This differs from the actual PZ, which is affected by stress redistribution during plastic flow. Fig. 5(a-c) shows the chronological growth of PZ ahead of the crack tip for β_{eq} = 0° (Mode II), β_{eq} = 84° (mixed-mode (I/II)), and β_{eq} = 90° (Mode-I) of the asymmetric TPB specimen, subjected to a range of applied loads. The crack-tip PZ shapes for each load step are merged in Figs. 5(a-c). The displacement scaling of asymmetric TPB specimens is set to zero in Fig. 5(a-c) to analyze the magnitudes and shape of the crack-tip PZ. From Fig. 5(a), it is clearly seen that the development of PZ contours takes place in the vertical direction (*i.e.*, along the ligament) for β_{eq}=0°. In this figure, the shape of PZ at the lower right of the crack is found to deviate from the expected normal shape due to the loading point at the crack tip. Fig. 5(b) reveals that the growth of the PZ takes place at an angle of stretch (θ to crack plane) between 0° and 90°. For β_{eq} = 90° (Mode I), the PZ grows horizontally (*i.e.*, perpendicular to the ligament) as shown in Fig. 5(c). From Fig. 5(a) for β_{eq} = 0° (Mode II), it is clearly seen that the PZ contours are more dominating at the loading rather than at the crack-tip. Hence, the applied load on the asymmetric TPB specimen under Mode II loading will not be distributed at the crack tip. This is because, for Mode II loading, the crack is exactly at the roller of the asymmetric TPB specimen.

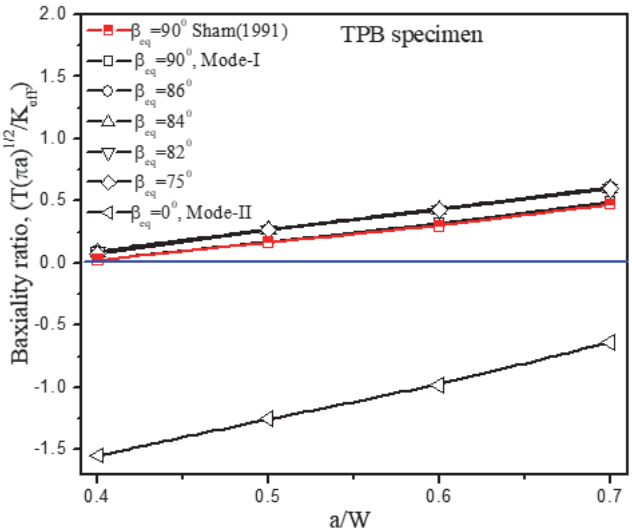

Figure 4: Variation of Biaxility ratio (*B*) vs. a/W for different βeq.

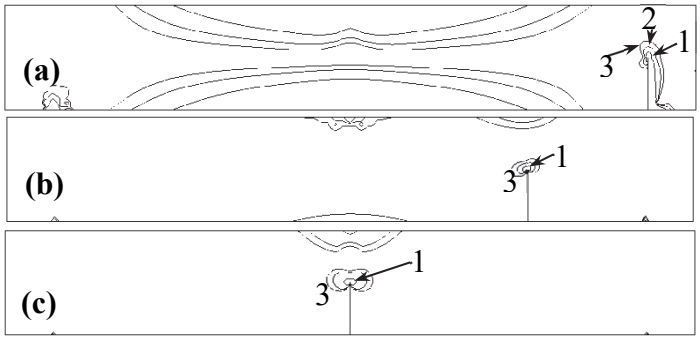

Figure 5: Sequential development of plastic zone for various applied loads. Number 1, 2, 3 indicates the plastic zone for applied load **(a)** 4, 6 and 8kN for β_{eq}= 0°, **(b)** 1, 1.5 and 2 kN, for β_{eq} = 85°, **(c)** 0.5, 1 and 1.25 kN, for β_{eq} = 90°.

.

The growth and alteration of the crack-tip PZ for various β_{eq}, and a/W, typically for K_{eff} = 900 MPamm$^{1/2}$ in an asymmetric TPB specimen, are shown in Fig. 6, with the contours are superimposed. The plastic contours that are superimposed in Fig. 6 for β_{eq}=90° (Mode I) to 0° (Mode II) of the asymmetric TPB specimen are Von-Mises stress distribution, typically for yield stress 155 MPa [20] of the material. The contour lines appear to cross due to the superposition of multiple plastic zone boundaries for different loading angles (β_{eq} = 0°, 75°, 82°, 84°, 86°, and 90°) plotted. For the same value of K_{eff} = 900 MPamm$^{1/2}$ from Fig. 6, one can observe that the size of PZ is larger for β_{eq} = 0° (Mode II) compared to larger β_{eq}, and it will be smaller PZ for β_{eq} = 90° (Mode I). The shapes of the crack tip PZ for various β_{eq} of an asymmetric TPB specimen obtained from FE analysis will closely match with the theoretical PZ shapes presented in Eqn. (5), as shown in Fig. 7, typically for K_{eff} =900 MPamm$^{1/2}$. Earlier work demonstrated that the size of the crack tip PZ depends on the materials fracture toughness [9, 19]. So, based on the magnitude of the PZ form Fig. 6 and Fig. 7, the result clearly reveals that the loading for β_{eq} = 90° is more dangerous than other β_{eq} for the asymmetric TPB specimen. In the present work, the major crack-tip PZ parameters will concentrate on i) the measurement of GMPZR and (ii) the crack initiation angle θ_o at which GMPZR occurs, are schematically exemplified in Fig. 7.

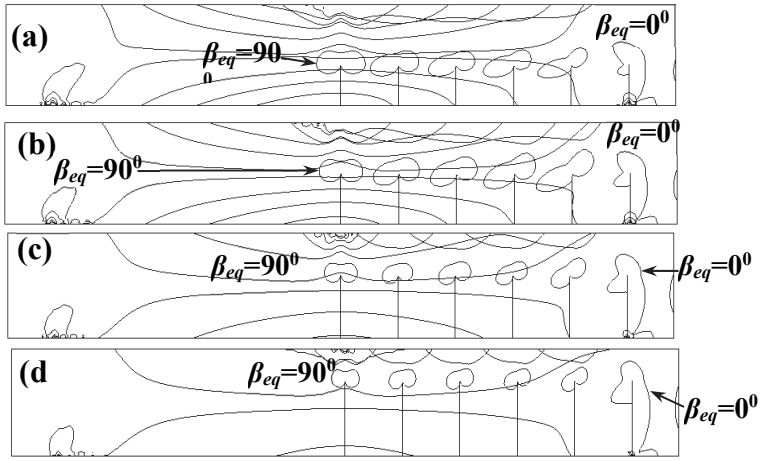

Figure 6: Typical plastic zone contours computed for various a/W7and β_{eq} for applied K_{eff}=900 MPa mm$^{1/2}$.

For the analysis of GMPZR with normalized K_{eff}, the GMPZR will be normalized by thickness (h). The plot of normalized GMPZR *vs.* normalized K_{eff} is shown in Fig. 8. This Figure demonstrates that the variation is linear, and the slope estimated will be nearly equal across different a/W and β_{eq}. Form Fig. 8, the normalized GMPZR *vs.* normalized K_{eff} shows a proportional relationship for all a/W and β_{eq} of the asymmetric TPB specimen. Hence, one can establish the proportionality constant by fitting a straight-line equation to all the normalized GMPZR data. The estimated slope for the linear fit is 0.0035 for the asymmetric TPB specimen of various a/W and β_{eq}. Mathematically, the relation between normalized GMPZR (r_{min}) and normalized K_{eff} can be given as:

$$\frac{\frac{r_{\min}}{h}}{\frac{K_{eff}}{\sigma_y\sqrt{h}}} = 0.0035 \tag{11}$$

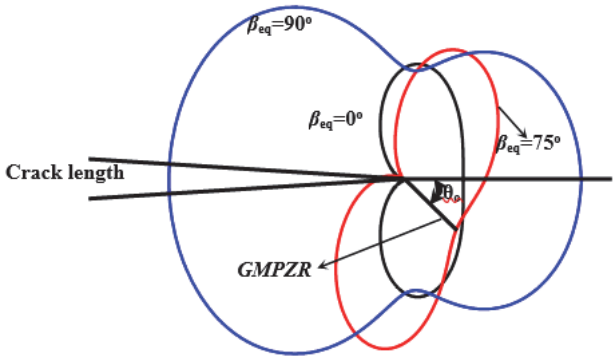

Figure 7: Sequential development of plastic zone obtained by analytical of various β_{eq} for applied K_{eff}=900 MPa mm$^{1/2}$.

For an asymmetric TPB specimen with any a/W and β_{eq}, if K_{eff}, σ_y, and h are known in Eqn. (11), one can estimate the value of GMPZR, or vice versa. Consequently, the obtained Eqn. (11) can be of great use in GMPZR crack initiation criteria:

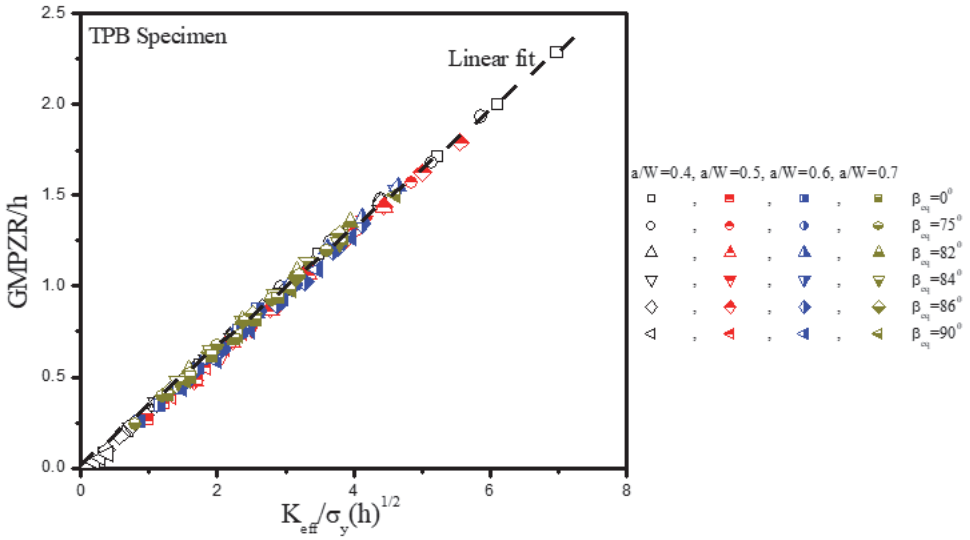

Figure 8: Variation of GMPZR/h *vs.* $K_{\text{eff}}/\sigma_y(h)^{1/2}$ for various β_{eq} and a/W ratios.

The crack initiation angle (θ_o) is studied as a function of the equivalent loading (β_{eq}) angle. The variation of θ_o *vs.* β_{eq} obtained in this analysis for various applied loads is compared with the theoretical GMPZR criterion (Eq. (5)), similar results of Khan and Khraisheh [19], Bian and Kim [9], MTS criterion [27], and GMTS criteria [16] in Fig. 9.

Fig. 9 shows that the FEA-measured value of θ_o for the asymmetric TPB specimen decreases from 83° to 0° as β_{eq} varies from 0° to 90°. From Fig. 9, it is clear that the FEA-measured θ_o *vs.* β_{eq} for the asymmetric TPB specimen is independent of the applied loads. Due to measurement of θ_o difficulties in FEA analysis for an asymmetric TPB specimen, one can observe a slight variation in θ_o for various β_{eq}. The FE results of θ_o *vs.* β_{eq} shown in Fig. 9 are in good agreement with the theoretical results estimated by Eq. (5). In Fig. 9, the measured values of θ_o from FE analysis of asymmetric TPB specimen are closely matched with the analytical results of Khan and Khraisheh [19], and about 5°-10° higher than that of Bian and Kim [9] results for β_{eq} between 50°-70°. This deviation in results between the FE and the Bian and Kim [9] work may be attributed to the specimen geometry (θ_o in the earlier work [9] was obtained on a CTS specimen). In Fig. 9, the asymmetric TPB FE results for θ *vs.* β_{eq} were compared with the experimental results for a CTS mixed-mode (I/II) fracture specimen as reported

in the work of Bian and Kim [9]. The nature of variation is similar, but due to differences in specimen geometry, the present FE results for the asymmetric TPB specimen deviate more from available experimental results [9]. In Fig. 9, it is clearly observed that the FE results of the asymmetric TPB specimen will deviate from the MTS criterion [27], and the GMTS criterion [16] for the variation of θ_o *vs.* β_{eq}. This dissimilarity between the present FE criterion and the MTS [27] and GMTS [16] criteria results from the measurement of θ_o. In the present FE results, the measurement of θ_o is in accordance with the von-mises criterion, but in the MTS [27] and GMTS [16] criteria, the measurement of θ_o is based on the presence of a maximum tangential stress ahead of the crack tip.

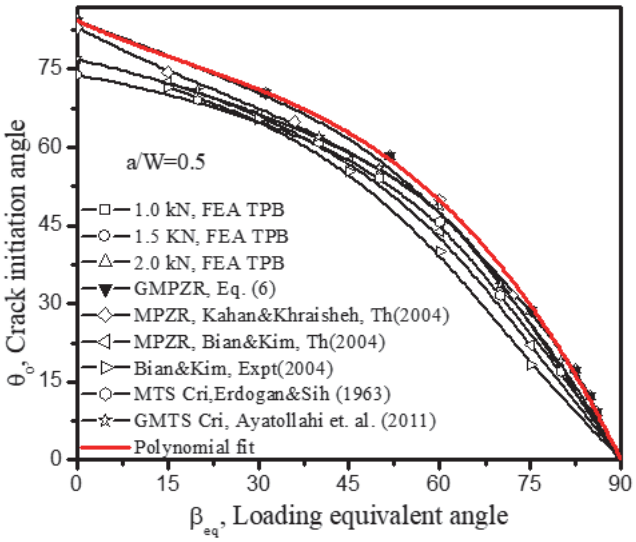

Figure 9: Variation of θ_o *vs.* β_{eq} for various applied loads.

In this work, a relation between θ_o (crack initiation angle) and β_{eq} (equivalent loading angle) is proposed, which will be helpful in the application of GMPZR theory to asymmetric TPB specimens. To obtain a relation between θ_o and β_{eq}, the present FE results in Fig. 9 are fit with a third-order polynomial, selected as it yields a fit of 0.999. The polynomial fit, shown in Fig. 9 as a red line, exhibits excellent agreement with the present FE results. The obtained analytical third-order polynomial expression is:

$$\theta_o = 82.561 - 0.634\left(\beta_{eq}\right) + 0.0133\left(\beta_{eq}\right)^2 - 1.833\text{E-}4\left(\beta_{eq}\right)^3 \tag{16}$$

where θ_o is the crack initiation angle, and β_{eq} is the equivalent loading, respectively. The similar plots of θ_o *vs.* β_{eq} are also plotted for various specimen a/W ratios in Fig. 10. It is clear from Fig. 9 and Fig. 10 that the variation of θ_o *vs.* β_{eq} is independent of loading and a/W ratios. The third-order polynomial fit for these results yields the similar to Eqn. (16).

The results presented in this study and the proposed Eqns. (15) and (16) are useful to researchers and industrial scientists to predict the magnitude of GMPZR and θ_o (crack initiation angle) for TPB specimens for various a/W ratios by only knowing the magnitude of K_I and K_{II} in association with Eqns. (15) and (16). The analytical equations can be used to estimate K_I and K_{II} because of negligible errors in estimating of FE and in the analytical results for the stress intensity factor, thereby making the proposed formulations simpler and easier to apply.

The effect of T-stress on θ_o estimated from the GMPZR criterion for various a/W ratios was studied through the variation of biaxiality ratio (B) *vs.* crack initiation angle (θ_o) as shown in Fig. 11. From Fig. 11, it is observed that the variation of B increases for $\theta_o \geq 0^o$ to 15^o, and it is constant up to 70^o, and it gradually decreases for $\theta_o \leq 71^o$ to 83^o. The results from Fig. 11 clearly indicate that the crack initiation angle will be affected more for Mode II loading (θ_o=83^o) compared to other combined (Mode I + Mode II) and Mode I loading conditions.

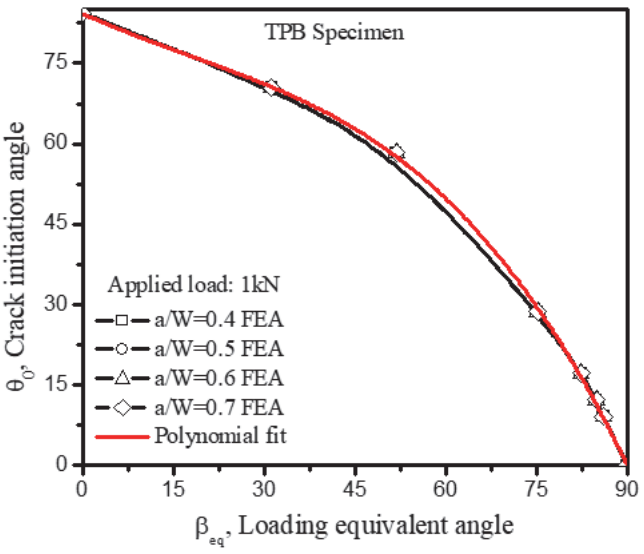

Figure 10: Variation of θ_o *vs.* β_{eq} for various a/W ratios.

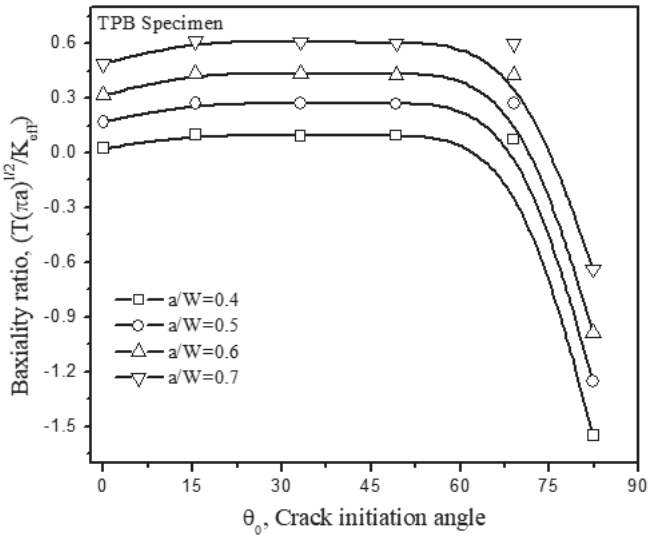

Figure 11: Variation of B *vs.* θ_o for various specimen a/W ratios.

CONCLUSIONS

The following conclusions are drawn from the present study:

1. For β_{eq}=90° (Mode I), the asymmetric TPB specimen undergoes earlier fracture compared to 0°≤β_{eq}<90° (mixed-mode (I/II) and Mode II).
2. For the asymmetric TPB specimen, the variation of GMPZR is linear with K_{eff} and is independent of the β_{eq} and a/W. The estimated crack initiation angles for various equivalent loading angles are independent of the applied load and the specimen a/W ratio.
3. The relationships between GMPZR and K_{eff}, and between θ_o and β_{eq} are proposed for an asymmetric TPB specimen. They are useful for estimating the magnitudes of GMPZR and θ_o (crack initiation angle) for various a/W using only the equivalent loading angle.
4. The asymmetric TPB specimen geometry will affect higher-order terms, which, in turn, will affect θ_o. Consequently, θ_o will be affected more by Mode II loading than by combined (Mode I + Mode II) or Mode I Loading conditions.
5. The present work can be extended to elastic–plastic finite element analyses that consider parameters (stress redistribution and crack-tip triaxiality), allowing investigators to validate the proposed GMPZR criterion beyond the small-scale yielding regime.

REFERENCES

[1] Miao, X., Huang, X., Ding, P., Li, Y. and Li, S. (2023). The study of mixed mode fatigue crack growth mechanism of 25CrNiMo compact tensile specimens by experiment and finite element simulation, Proc. Inst. Mech. Eng., Part C: J. Mech. Eng. Sci., 237(12), pp. 2887–2900. DOI: https://doi.org/10.1177/09544062221141846.

[2] Giannella, V. and Perrella, M. (2019). Multi-axial fatigue numerical crack propagation in cruciform specimens, Fract. Struct. Integr., 13(48), pp. 639–647. DOI: https://doi.org/10.3221/IGF-ESIS.48.61.

[3] Mokhtari, M., Lopez-Crespo, P., Moreno, B. and Zanganeh, M. (2015). Some experimental observations of crack-tip mechanics with displacement data, Fract. Struct. Integr., 9(33), pp. 143–150. DOI: https://doi.org/10.3221/IGF-ESIS.33.18.

[4] Song, W., Yan, W., Cui, Z., Chen, X. and Wu, H. (2025). Investigating the fracture behaviors of asphalt mixtures at the intermediate temperature considering the detection of crack initiation, Eng. Fract. Mech., 316, 110892. DOI: https://doi.org/10.1016/j.engfracmech.2025.110892.

[5] Chen, C., Cheok, E.W.W. and Qian, X. (2026). DIC-based J-integral quantification for through-thickness crack in CHS joints, Eng. Struct., 353, 122243. DOI: https://doi.org/10.1016/j.engstruct.2026.122243.

[6] Perez, N. (2016). Crack tip plasticity, In: Fracture Mechanics. Springer, Cham., pp. 187–225. DOI: https://doi.org/10.1007/978-3-319-24999-5_5.
[7] Breitbarth, E. and Besel, M. (2017). Energy based analysis of crack tip plastic zone of AA2024-T3 under cyclic loading, Int. J. Fatigue, 100, pp. 263–273. DOI: https://doi.org/10.1016/j.ijfatigue.2017.03.029.
[8] Wu, G., Wang, W. and Peng, S. (2024). Analytical solution of the stress field and plastic zone at the tip of a closed crack, Front. Earth Sci., 12, 1370672. DOI: https://doi.org/10.3389/feart.2024.1370672.
[9] Bian, L.-C. and Kim, K.S. (2004). The minimum plastic zone radius criterion for crack initiation direction applied to surface cracks and through-cracks under mixed mode loading, Int. J. Fatigue, 26(11), pp. 1169–1178. DOI: https://doi.org/10.1016/j.ijfatigue.2004.04.006
[10] Perez, N. (2016). Mixed-mode fracture mechanics, In: Fracture Mechanics. Springer, Cham. pp. 289–325. DOI: https://doi.org/10.1007/978-3-319-24999-5_8.
[11] Christodoulou, P.I. and Kermanidis, A.T. (2023). A Combined Numerical–Analytical Study for Notched Fatigue Crack Initiation Assessment in TRIP Steel: A Local Strain and a Fracture Mechanics Approach, Metals, 13(10), 1652. DOI: https://doi.org/10.3390/met13101652.
[12] Shahani, A. and Tabatabaei, S. (2009). Effect of T-stress on the fracture of a four point bend specimen, Materials, 30(7), pp. 2630–2635. DOI: https://doi.org/10.1016/j.matdes.2008.10.031.
[13] Wu, Q.H., Xie, C.L., Xie, Y.S., Zhao, Y.L., Li, X.F., Liu, J. and Weng, L. (2022). Extending application of asymmetric semi-circular bend specimen to investigate mixed mode I/II fracture behavior of granite, J. Cent. South Univ., 29(4), pp. 1289–1304. DOI: https://doi.org/10.1007/s11771-022-4989-6.
[14] Stepanova, L.V. and Belova, O.N. (2023). Stress intensity factors, T-stresses and higher order coefficients of the Williams series expansion and their evaluation through molecular dynamics simulations, Mech. Adv. Mater. Struct., 30(19), pp. 3862–3884. DOI: https://doi.org/10.1080/15376494.2022.2084800.
[15] Yakoubi, K., Montassir, S., Moustabchir, H., Elkhalfi, A., Scutaru, M.L. and Vlase, S. (2022).T-stress evaluation based cracking of pipes using an extended isogeometric analysis (X-IGA), Symmetry, 14(5), 1065. DOI: https://doi.org/10.3390/sym14051065.
[16] Ayatollahi, M., Smith, D. and Pavier, M. (2011). Characterizing mixed-mode brittle fracture using near crack tip stress fields, In: Proceedings of First IJFatigue & FFEMS Joint Workshop, Gruppo Italiano Frattura, 9–16. ISBN: 8895940350.
[17] Nazarali, Q. and Wang, X. (2011). The effect of T-stress on crack-tip plastic zones under mixed-mode loading conditions, Fatigue Fract. Eng. Mater. Struct., 34(10), pp. 792–803. DOI: https://doi.org/10.1111/j.1460-2695.2011.01573.x.
[18] Miao, X.T., Zhou, C.Y., Lv, F. and He, X.H. (2017). Three-dimensional finite element analyses of T-stress for different experimental specimens, Theor. Appl. Fract. Mech., 91, pp. 116–125. DOI: https://doi.org/10.1016/j.tafmec.2017.04.018.
[19] Khan, S.M. and Khraisheh, M.K. (2004). A new criterion for mixed mode fracture initiation based on the crack tip plastic core region, Int. J. Plast. 20(1), pp. 55–84. DOI: https://doi.org/10.1016/S0749-6419(03)00011-1.
[20] Ma, F., Sutton, M.A. and Deng, X. (2001). Plane strain mixed mode crack-tip stress fields characterized by a triaxial stress parameter and a plastic deformation extent based characteristic length, J. Mech. Phys. Solids, 49(12), pp. 2921–2953. DOI: https://doi.org/10.1016/S0022-5096(01)00018-7.
[21] Yazdani, M. and Yavari, A. (2024). Scaled boundary finite element method for calculating the J-integral based on LEFM. Mech. Adv. Mater. Struct., 31(16), pp. 3817–3828. DOI: https://doi.org/10.1080/15376494.2023.2185707.
[22] Kudari, S.K., Maiti, B. and Ray, K.K. (2007). The effect of specimen geometry on plastic zone size: a study using the J integral, J. Strain Anal. Eng. Des., 42(3), pp. 125–136. DOI: https://doi.org/10.1243/03093247JSA252.
[23] He, M. and Hutchinson, J. (2000). Asymmetric four-point crack specimen, J. Appl. Mech., 67(1), pp. 207–209. DOI: https://doi.org/10.1115/1.321168.
[24] Murakami, Y. (Ed.) (1987). Stress Intensity Factors Handbook, 1st ed., Pergamon Press, Oxford, UK.
[25] Tyrymov, A.A. (2022). Numerical simulation of T-stresses and stress biaxiality factor for a centrally cracked specimen under mixed boundary conditions, J. Appl. Mech. Tech. Phys., 63(7), pp. 1264–1271. DOI: https://doi.org/10.1134/S002189442207015X.
[26] Sham, T.L. (1991). The determination of the elastic T-term using higher order weight functions, Int. J. Fract., 48(2), pp. 81–102. DOI: https://doi.org/10.1007/BF00018392.
[27] Erdogan, F. and Sih, G. (1963). On the crack extension in plates under plane loading and transverse shear. J. Basic Eng., 85(4), pp. 519–525. DOI: https://doi.org/10.1115/1.3656897.